

Processes of India's offshore summer intraseasonal sea surface temperature variability

K. Nisha¹, M. Lengaigne^{1,2}, V.V. Gopalakrishna,¹ J. Vialard², S. Pous², A.-C. Peter², F. Durand³, S.Naik¹

1. *NIO, CSIR, Goa, India*

2. *LOCEAN, IRD/CNRS/UPMC/MNH, Paris, France*

3. *LEGOS, IRD/CNRS/CNES/UPS, Toulouse, France*

Corresponding author address:

Nisha Kurian

Physical Oceanography Division, National Institute of Oceanography, Dona Paula. Goa
India – 403004; E-mail: neeshakurian@gmail.com

Abstract

Active and break phases of the Indian summer monsoon are associated with 30-90 days Sea Surface Temperature (SST) fluctuations in the Arabian Sea and Bay of Bengal. Mechanisms responsible for basin-scale SST variations have previously been discussed, but the maxima of intraseasonal SST variability are actually located in three specific offshore regions: the South-Eastern Arabian Sea (SEAS), the Southern Tip of India (STI) and the North-Western Bay of Bengal (NWBoB). In the present study, we use an eddy-permitting $\frac{1}{4}^\circ$ regional Ocean Circulation Model to investigate mechanisms of this offshore intraseasonal SST variability. Modelled climatological mixed layer and upper thermocline depth are in very good agreement with estimates from 3 repeat XBT transects perpendicular to the Indian Coast. The model intraseasonal forcing and SST variability agree well with observed estimates, although modelled intraseasonal offshore SST amplitude is underestimated by 20-30%. Surface heat flux variations drive a large part of the intraseasonal SST variations along the Indian coastline. Oceanic processes have contrasted contributions depending of the region. In the SEAS, this contribution is very small because intraseasonal wind variations are essentially cross-shore, and thus not associated with significant upwelling intraseasonal fluctuations. In the STI, vertical advection associated with Ekman pumping contributes to $\sim 30\%$ of the SST fluctuations. In the NWBoB, vertical mixing diminishes the effect of the atmospheric heat flux perturbations by 40%. Simple slab ocean model integrations show that the amplitude of these intraseasonal SST signals is not very sensitive to the heat flux dataset used, but more sensitive to mixed layer depth.

Keywords: Indian Ocean, Intraseasonal variability, Sea Surface Temperature, Regional Ocean Model, oceanic and atmospheric processes

1. Introduction

Atmospheric intraseasonal variability in the northern Indian Ocean during summer is largely dominated by two phenomena: the 10-20 days westward propagating Quasi Biweekly Mode (Chatterjee and Goswami 2004) and the 30-90 days northward propagating active and break phases of the monsoon (Goswami and Ajaya Mohan 2001). The Sea Surface Temperature response to the latter phenomenon is larger (e.g. Sengupta et al. 2001; Duvel and Vialard 2007) and will be the focus of the present paper. Active phases are characterized by increased convection and rainfall over India, eastern Arabian Sea and the Bay of Bengal, as well as a strengthening of the monsoon jet while break phases are characterized by increased convection and rainfall south of tip of India, a deflection of the low level jet southward and decreased winds over the Arabian Sea, India and the Bay of Bengal (e.g. Goswami and Ajaya Mohan 2001; Webster et al. 1998; Joseph and Sijikumar 2004).

These intraseasonal atmospheric signals over the northern Indian Ocean largely arise from coupling between large-scale atmospheric dynamics and deep convection (Lawrence and Webster 2002; Goswami 2005) and impact surface wind and downward solar irradiance, therefore inducing intraseasonal fluctuations of net heat and momentum fluxes at the ocean surface. Analysis of microwave SST measurements revealed that these intraseasonal flux perturbations result in relatively large SST signals (1-2°C) in the northern Bay of Bengal and South China Sea (Sengupta et al. 2001; Vecchi and Harisson 2002; Duvel and Vialard 2007; Vinayachandran et al. 2012) but also in the Somali and Oman upwelling regions (Duvell and Vialard 2007; Roxy and Tanimoto 2007; Joseph and Sabin 2008; Vialard et al. 2012) and close to the Southern tip of India (Rao et al. 2006; Ganer et al. 2009). These SST signals propagate northward along with atmospheric convection and surface flux perturbations (Vialard et al. 2012).

Several modelling studies have assessed the mechanisms involved in the SST response to monsoon active and break phases over the Bay of Bengal (Fu et al. 2003; Waliser et al. 2004; Bellon et al. 2008; Duncan and Han 2009; Vialard et al. 2012; Vinayachandran et al. 2012). Among these studies, there is a reasonable consensus in designating air-sea fluxes as the main driver of large-scale intraseasonal SST variations in the northern Bay of Bengal, with a weaker and variable contribution from exchanges with the ocean subsurface (through vertical mixing, vertical advection and entrainment). Fewer studies (Rao et al. 2006; Ganer et al. 2009; Duncan and Han 2009; Vialard et al. 2012) have discussed the processes involved in the SST fluctuations associated with monsoon active and break phases in the Arabian Sea, and the emerging picture is somewhat different. Using

observations, Rao et al. (2006) show pronounced intraseasonal cooling episodes in the so-called Mini Cold Pool (henceforth MCP) off the southern tip of India and suggested that the MCP is primarily caused by wind-driven divergence in the near surface circulation. Using a simple 2.5-layer thermodynamical ocean model, Ganer et al. (2009) however stressed out that low incoming shortwave radiation and strong latent heat losses were also responsible for these cooling in addition to wind induced Ekman pumping, but did not perform any quantitative estimation. Duncan and Han (2009) find an equivalent influence of intraseasonal variations of latent heat flux (driven by changes in wind speed) and of wind stress to the summertime intraseasonal SST variations in Central and Southern Arabian Sea (their Fig. 6). Using a coarse resolution regional ocean model, Vialard et al. (2012) suggested that wind-stress intraseasonal variations are the primary factor driving 30-90 days intraseasonal SST fluctuations, through modulation of oceanic processes (entrainment, mixing, Ekman pumping, lateral advection) in upwelling regions of the Arabian sea (Somalia, Oman and STI upwellings).

Most previous studies investigated processes controlling SST variations over rather large regions but did not specifically address regions where the strongest SST variations are found (i.e. in upwelling regions). Aside from the Oman and Somalia upwelling regions where the largest summertime intraseasonal SST fluctuations occur, Indian offshore regions also exhibit large SST variations, which amplitudes are considerably larger than those found in the central parts of the Bay of Bengal and Arabian Sea, especially in the South-Eastern Arabian Sea (SEAS), near the Southern Tip of India (STI) and in the North-Western Bay of Bengal (NWBOB, see Figure 1a for these regions definitions). There are mainly two motivations to study these intraseasonal SST variations maxima. First, two of these regions (SEAS and NWBoB) display the highest climatological precipitation during summer monsoon, and very high background SST. As the result of intraseasonal variations, SST is consistently roaming around the 28.5°C threshold for deep atmospheric convection, (Gadgil et al. 1984), with potential significant impact on the local convection and rainfall. In addition, several studies have underlined the very intense chlorophyll blooms that can happen near the coasts of India due to strong wind variations associated with tropical cyclones (e.g. Vinayachandran and Mathew 2003, Maneesha et al. 2010), with a potential significant impact on fishery production. By analogy, intraseasonal modulation of the upwelling by local wind may well also affect biogeochemistry and fish populations significantly in these offshore regions.

The goal of the present study is to investigate the mechanisms driving intraseasonal SST signals in Indian offshore regions (Figure 1a). To that end, we will use an eddy permitting $\frac{1}{4}^\circ$ regional ocean model, that should allow to resolve details of the offshore processes (e.g. offshore

upwelling) better than in the previous studies of Vialard et al. (2012) (1° resolution) or Duncan and Han (2009) ($1/2^\circ$ resolution) and in a similar way to Vinayachandran et al. (2012). Section 2 describes the observational data sets and the modelling framework. A validation of key model parameters for resolving intraseasonal SST fluctuations is presented in Section 3. Section 4 describes the respective contribution of oceanic and atmospheric processes in governing intraseasonal SST variability along the Indian coast. Finally, Section 5 summarizes the results and discusses their implications.

2. Datasets and methods

a. Observations

The $1/4^\circ$ daily resolution optimally interpolated TMI (Tropical rainfall measuring mission-Microwave Instrument) SST data from Remote sensing systems (RSS) has been used owing to its ability to “see” through clouds (Wentz et al. 2000). It is available from December 1997 to present.

The mixed layer depth and depth of the upper thermocline are two important parameters in the upper ocean response to forcing. We thus validate those fields in the model by comparison with the mixed layer depth climatology from de Boyer Montegut et al. (2004) and the 25°C isotherm depth climatology derived from World Ocean Atlas 2009 (WOA09, Locarnini et al. 2010). These datasets however have a rather coarse resolution and may not properly resolve details within the offshore region of India. We therefore also use repeated XBT measurements performed by passenger ships that ply between India and overseas islands, and sample India offshore margins. This long-term observational program, supported by the Ministry of Earth Sciences of India, will allow us validating details of the model behaviour in the offshore regions. Along the west coast, the XBT transect is being repeated at near fortnightly intervals since 2002 between Kochi and Lakshadweep islands (see tracks on Figure 4a). Along the east coast, the XBT transect is being repeated at bi-monthly intervals since 1990 and at monthly intervals since 2006 between Chennai and Andaman Island and Andaman Island and Kolkata (see tracks on Figure 4a). During each cruise, 10 to 13 XBTs are deployed in each transect respectively at 50 km and 100 km intervals, typically sampling the upper 760 m. The XBT data are processed and quality controlled following procedures described in Bailey et al. (1994).

Model heat flux is validated against two recent datasets, largely derived from reanalysis products: OAFflux (Yu and Weller 2007) and Tropflux (Praveen Kumar et al. 2010). While TropFlux is largely derived from the ECMWF Interim Re-Analysis (ERA-I, Dee and Uppala 2009), OAFflux surface fluxes are obtained from a blend of various satellite retrievals and re-analysis products

through a variational method. TropFlux also provides estimates of wind stress, which perform better than other available products at intraseasonal timescale, when compared against in situ moored buoy estimates (Praveen Kumar et al. 2012).

b. Model description and forcing strategy

The model configuration that we use is based on the NEMO ocean general circulation modeling system (Madec 2008), and is a sub-domain from the global $1/4^\circ$ resolution (i.e. cell size ~ 25 km) ORCA025 coupled ocean/sea-ice model configuration described by Barnier et al. (2006) that extends from 26.75°E to 142.25°E and from 33.2°S to 30.3°N . The vertical grid has 46 levels, with a resolution ranging from 5 m at the surface to 250 m at the bottom. It uses a partial step representation of the bottom topography and a momentum advection scheme which both yield significant improvements (Penduff et al. 2007; Le Sommer et al. 2009). The bathymetry is a smooth combination of U.S. Department of Commerce, National Oceanic and Atmospheric Administration, National Geophysical Data Center 2-minute Gridded Global Relief Data (ETOPO2v2) and General Bathymetric Chart of the Oceans data over shelves. Vertical mixing is modelled with a prognostic turbulent kinetic energy scheme, with background vertical diffusion and viscosity of $10^{-5} \text{ m}^2\text{s}^{-1}$ and $10^{-4} \text{ m}^2\text{s}^{-1}$, respectively (Blanke and Delecluse 1993; Madec 2008). Additional subgrid-scale mixing parameterizations include a bi-Laplacian viscosity and an iso-neutral Laplacian diffusivity.

The African continent closes the western boundary of the domain. The oceanic portions of the eastern, northern and southern boundaries are radiative open boundaries (Treguier et al. 2001) constrained with a 150 days time-scale relaxation to 5-day-average velocities, temperature and salinity from an interannual global $1/4^\circ$ simulation (Dussin et al., 2009). This simulation is a product of the DRAKKAR hierarchy of global configurations (Drakkar Group, 2007), and has been extensively validated in the Indo-Pacific regions (Lengaigne et al. 2012, Keerthi et al. 2012, Nidheesh et al. 2012). The model starts from the World Ocean Atlas temperature and salinity climatologies (Locarnini et al. 2010) at rest and is forced from 1990 to 2007 with the Drakkar Forcing Set #4 (DFS4) described in Brodeau et al. (2010). The starting point of DFS4 is the CORE dataset developed by Large and Yeager (2004). The CORE bulk formula is used to compute latent and sensible heat fluxes, with surface atmospheric variables (air temperature, humidity and winds at 10 m) from the ERA40 reanalysis (Uppala et al. 2005) and European Centre of Medium-range Weather Forecasts (ECMWF) analysis after 2002. Radiative fluxes are similar to those from the CORE v1 dataset, i.e. based on corrected ISCCP-FD surface radiations (Zhang et al. 2004) while precipitation data are similar to those proposed by Large and Yeager (2004), namely GXGXS, based on a blending of several satellite products, including two of the most widely used datasets: GPCP

(Huffman et al. 1997) and CMAP (Xie and Arkin 1997). All atmospheric fields are corrected to avoid temporal discontinuities and remove known biases (see Brodeau et al. 2010 for details). Continental runoffs are taken from Dai and Trenberth (2002) monthly climatology. To avoid an artificial model drift, the sea surface salinity is nudged towards monthly-mean climatological values with a relaxation timescale of 300 days for a 50m-thick mixed layer (Griffies et al., 2009). The nudging timescale used will allow simulating realistic climatological haline stratification, a key feature of the Bay of Bengal, without altering the salinity stratification on intraseasonal timescales. This experiment successfully reproduces observed boreal winter intraseasonal SST variations in the thermocline ridge region and Northwest Australian basin (Vialard et al. 2012).

c. Methods

We use the model mixed layer heat budget equation to understand processes of SST intraseasonal variations. The terms contributing to the heat budget in the ocean mixed layer are calculated online and stored. The mixed layer depth (hereafter MLD) is defined as the depth where the vertical density is 0.01 kg.m^{-3} higher than the surface density. A lower model MLD criterion has to be applied compared to observations (0.03 kg.m^{-3}) because the model shortwave forcing does not account for any diurnal variability (de Boyer Montégut et al. 2004). In the model, the mixed layer temperature evolution equation reads:

$$\partial_t T = - \underbrace{\langle u \partial_x T + v \partial_y T + w \partial_z T \rangle}_a + \underbrace{\langle D_l(T) \rangle}_b - \underbrace{\frac{1}{h} \frac{\partial h}{\partial t} (T - T(z=h))}_c + \underbrace{\frac{(k \partial_z T)(z=h)}{h}}_d + \underbrace{\frac{Q^* + Q_s(1-F(z=h))}{\rho_0 C_p h}}_e \quad (1)$$

where T is the model temperature in the mixed layer, (u, v, w) the components of ocean currents, $D_l(T)$ the lateral diffusion operator, k the vertical diffusion coefficient, and h the time varying mixed layer depth. Brackets denote the vertical average over the mixed layer h . (a) is the advection, (b) the lateral diffusion, (c) is the entrainment/detrainment, (d) the vertical diffusion flux at the mixed layer base, and (e) is heat flux forcing of the mixed layer. Q_s is the solar heat flux; Q^* the non-solar heat fluxes: sensible, latent, radiative heat fluxes; and $F(z=h)$ the fraction of surface solar irradiance that penetrates below the mixed layer.

We have computed online the values for each term of equation (1) and saved them as 5 day averages. These tendency terms has been first filtered within the 30-110 days band before being temporally integrated. To check the consistency of our method, we have verified that the sum of all

the integrated intraseasonal filtered tendency terms is equal to the intraseasonally filtered SST output from the model. We will use this heat budget calculation to infer the respective contribution of these processes to the amplitude of intraseasonal SST perturbations along the Indian coastlines. The term (b) for lateral diffusion is negligible at these timescales and will not be discussed in the following. (c) and (d) are grouped together in a vertical processes term and referred to as MIX; (e) the surface forcing term is referred to as FLX; (a) the advection term is referred to as ADV.

In complement of the model full surface layer heat budget, we will also provide diagnostics from a much simpler bulk mixed layer model, given by:

$$\partial_t T = \frac{Q_{net}}{\rho_0 C_p h_c} \quad (2)$$

Attention l'équation (2) n'apparait pas sur mon word : vérifier qu'elle apparait bien sur le pdf généré par le journal lors de la soumission

where $Q_{net}=Q^*+Q_S$ is the net surface heat flux and h_c is a seasonal mixed layer depth climatology, obtained either from observations (de Boyer Montégut et al. 2004) or from the model climatology. Previous studies have indeed shown that such a simple model (that neglects both penetrative solar heat flux, intraseasonal mixed layer depth fluctuations and processes other than surface forcing) reproduces intraseasonal SST fluctuations reasonably well in the Bay of Bengal and STI regions (Vialard et al. 2012).

We isolate intraseasonal signals in the model and observations using time-filtering. We use 30-110 day filtering everywhere in this paper, using a simple filter based on Fourier filtering (the coefficients of the Fourier transform outside of the 30-110 day periods are set to zero, and the reverse transform is performed). We checked that using different filtering methods and different bandpass windows (e.g. the more classical 30-60 day window used for summer intraseasonal variability as in Goswami 2005 and Vialard et al. 2012, a 10-60 day filter) gave qualitatively similar and quantitatively close results in terms of the relative contributions of forcing, subsurface processes and lateral advection to intraseasonal variations of the SST in the three offshore regions that we consider.

In order to provide an overview of the typical signals associated with intraseasonal variations in each region, we define a normalized SST index in each region (the 30-110 day filtered average SST in the region, normalized by its June-September standard deviation). Lagged regressions of the box-averaged 30-110 day filtered parameters (e.g. wind, MLD, heat fluxes) within the box to this

index give an overview of the typical signals associated with intraseasonal SST fluctuations in each region (see, e.g. Figures 9 to 13). We also use regression to provide a quantitative estimate of the contribution of the various processes involved in the intraseasonal SST modulation. Time integrals of various terms in equation (1) filtered in the 30-110 day band (i.e. contributions of various processes, in °C) are regressed to the 30-110 day filtered average SST in the region, thus providing the contribution of each process (in %) to the total intraseasonal SST variations. These coefficients are computed for the summer season (June-September) and provided in Table 3. They can either be positive or negative for a process that acts to amplify or damp the total variability.

3. Model validation

a. Intraseasonal atmospheric forcing and offshore SST signature

The standard deviation of the 30-110 day filtered June-September SST from TMI and model is presented in Figure 1. Aside from the large-scale maxima of intraseasonal SST variability found along the Somali and Oman coast and the basin-scale signal found in the northern Bay of Bengal, local intraseasonal SST variability maxima are found along the Indian coast. In the following, we will focus on three specific regions indicated by the frames drawn on Figure 1: the western coast of India, encompassing the southeastern Arabian Sea (SEAS region; 73-77° E- 9-12° N), the southern tip of India (STI region; 75-78° E, 5-9° N) and the northwestern part of the Bay of Bengal (NWBoB; 80-85° E, 15-19° N). As shown on Figure 1b, the model reproduces reasonably well the spatial distribution of intraseasonal SST variability, although slightly underestimating its amplitude in these three regions. As pointed out by Vinayachandran et al. (2012), who see a similar underestimation, this could be due to the tendency of the TMI SST product to overestimate intraseasonal variations (Bhat et al. 2004).

Figure 2 provides a validation of the model heat and momentum fluxes intraseasonal variability in summer against Tropflux dataset. A strong jet across Arabian Sea, Indian subcontinent and Bay of Bengal characterizes monsoon active phases, while break phases display a southward-deflected jet, located above the equatorial Indian Ocean (Joseph and Sijikumar 2004). As shown in Figure 2, these basic features result in three maxima of intraseasonal momentum and heat fluxes: in the region of the low-level monsoon jet in the Arabian Sea, in the Bay of Bengal and in the equatorial Indian Ocean between 80°E and 90°E. The model accurately reproduces the spatial structure of this intraseasonal forcing, except maybe in the Somalia upwelling region, which is not a focus in this study.

While the model wind stress intraseasonal variability amplitude compares very favourably with

observations, there is a clear underestimation of the large-scale heat flux intraseasonal variability at the basin-scale. Since our study focuses mainly on the offshore-regions of India in the three boxes introduced above (SEAS, STI and NWBoB), table 1 provides a validation of the model net heat fluxes to the TropFlux (Praveen Kumar et al. 2012) and OAFLUX (Yu and Weller 2007) products in those regions. The difference between the model fluxes and either datasets is in general smaller than the differences between the two flux datasets. This suggests that the model heat flux intraseasonal variations are within observational uncertainties in those boxes. The correlation between the model and observed intraseasonal net heat fluxes in those boxes is also always larger than 0.79. Despite some underestimations over the open ocean, the model heat flux intraseasonal variability is hence well reproduced in the SEAS, STI and NWBoB regions. Figure 3 allows discussing the phase and amplitude agreement of modelled and observed SST intraseasonal fluctuations over the three aforementioned regions. The phase agreement of the model to observations is good, with a correlation of 0.82, 0.70 and 0.79 for SEAS, STI and NWBoB regions respectively. The amplitude of summer intraseasonal SST perturbations is however underestimated by ~20-30% with amplitude ratios to observations of 0.69, 0.81 and 0.73 for SEAS, STI and NWBoB, respectively. This underestimation may be due to issues with the TMI product, as previously mentioned, but may also be related to a misrepresentation of the upper ocean structure in these regions, an important factor controlling the amplitude of SST signature (Sengupta and Ravichandran 2001; Vialard et al. 2012). We will hence validate this background oceanic structure in detail in section 3.b.

b. Background oceanic structure

The depth of the upper thermocline controls the temperature of the water that can be upwelled to the surface. As discussed in Gopalakrishna et al. (2010), the depth of the 25°C isotherm (D25) in the SEAS is a good proxy for the thermocline depth, i.e. the strongest vertical gradient region. We have checked that this is also verified for the two other regions and hence use D25 as a proxy for thermocline depth in this manuscript. The mixed layer depth (MLD) is an important parameter because it sets the propensity of the surface layer to respond to atmospheric fluxes. In addition, several studies (e.g. Shenoi et al. 2002, de Boyer Montégut et al. 2007, Vinayachandran et al. 2012) have pointed out the potential importance of haline stratification in the upper ocean heat balance of the Bay of Bengal. We hence validate all those aspects in this section. Figure 4 provides a model-data comparison of the upper thermocline depth (estimated from the depth of the 25°C isotherm, D25) in the northern Indian Ocean during the June to September (JJAS) period, based on a climatology built from in-situ observations. Figure 5 compares the modelled MLD with the observed product of de Boyer Montégut et al. (2004). Figure 6 compares the modelled climatological SSS and

barrier layer thickness (BLT) with the climatologies from Chatterjee et al. (2012) and de Boyer Montégut et al. (2004), respectively.

The model reproduces the main features of the observed D25. The low-level monsoon jet in the Arabian Sea results in a deep D25 on its right hand side (~120 m) (owing to Ekman convergence). Conversely, it generates a much shallower D25 on its left (~40 m), due to Ekman divergence. The model also shows the signature of upwelling in the SEAS and in the Sri Lanka Dome region (Vinayachandran and Yamagata 1998). On the other hand, the model suffers from a bias in the eastern equatorial Indian Ocean where the D25 is about 40 m deeper than in the observations. Similarly, the model produces a distinct patch of deep D25 in the Great Whirl area (53°E, 8°N), which is not seen in the observed product. This may be linked with the too coarse resolution of the observation grid. These two regions, however, are not the focus of the present study and these biases are unlikely to affect the conclusions of this paper.

The mixed layer of the central Arabian Sea is generally deeper compared to central part of the Bay of Bengal due to the stronger winds in the Arabian Sea (Fig. 5, Prasad 2004). The model reproduces this contrast, with in particular a shallower MLD observed in the northern Bay of Bengal. However, model and observed MLD datasets disagree in offshore regions, where the model simulates a shallower MLD than the one inferred from the observational dataset. Offshore MLD values in the SEAS and NWBoB are about 15 m in the model but exceed 25 m in the observed dataset. This discrepancy could arise from a model deficiency in properly simulating the ocean stratification close to the coast, but may also be related to observational issues. Figure 5c shows a map of the number of profiles used to calculate the MLD climatology in this dataset. While the number of profiles in the central part of the Arabian Sea and Bay of Bengal is relatively large (between 10 and 25 per 2° by 2° box per month), very few observations are available in the offshore regions. The numerous missing values along the offshore regions are filled using an ordinary kriging method, (de Boyer Montégut et al. 2004) which could generate an overestimation of the MLD along the coasts in the observed dataset and consequently could explain the discrepancies between model and observed estimates.

The large-scale structures of SSS in the north Indian Ocean are in reasonable agreement with observations (Figure 6ab), with differences below 1 psu everywhere in the Bay, with the exception of the very northern portion of the Bay where the model simulates fresher than observed surface waters. This may either be due to a resolution mismatch between the two datasets (the horizontal resolution is 0.25° in the model against 2° in the observations), model deficiencies or sparse observations in this region (see figure 1 from Chatterjee et al. 2012). As far as barrier layer is concerned (Figure 6cd), the

sparse data coverage does not really allow validating the details of the model behaviour, but apart from spurious "localized" BLT in the western Arabian sea, the model seems to reproduce the large-scale patterns in the BoB with little barrier layer in the southwestern Bay and progressively increasing BLT toward the northern and eastern rim of the Bay. There is about 10-15 m BLT in the NWBoB region and no BL in the SEAS and STI in the model and observations.

While the validations above are reassuring when it comes to the open ocean climatology of the model, they provide no real insights to the offshore regions, which are the focus of this study. To specifically investigate this issue in the offshore ocean, we make use of the repeated XBT measurements performed in the offshore regions surrounding India along the three specific sections indicated on Figure 5a (i.e. in the SEAS and in the western and northern Bay of Bengal) and compare the seasonal cycle of the offshore IsoThermal Layer Depth (ITLD) and depth of the 25°C isotherm estimated from this dataset to the model outputs. ITLD calculations are in this case performed based on a temperature criterion (the depth where the temperature reaches SST-0.2°C) due to the lack of subsurface salinity data along these transect. During the monsoon season barrier layer is virtually absent along the coast of India except the northern part of PK transect where barrier of ~10-20 m depth can be found (Thadathil et al. 2008, figure 6) and hence it is unlikely that salinity stratification strongly affects the mixed layer depth during the summer season.

The ITLD climatology for the SEAS region (Figure 7b) shows a contrasted evolution from the coast to the open ocean. An annual periodicity dominates the ITLD variability along the coast: the ITLD shoals during spring and summer reaching 10 m depth in August and deepens during the later part of year, reaching a 50 m maximum depth in December. In contrast, away from the coast, the ITLD displays a semi-annual periodicity, with a shoaling in spring and fall, a deepening in summer and winter (maximum in August). As suggested by Gopalakrishna et al. (2010), this east-west contrast may be attributed to different mechanisms controlling the ITLD seasonal variations: within the offshore waveguide, the ITLD changes are largely driven by the thermocline vertical movements, whereas the ITLD evolution towards the western edge of the transect are more affected by the buoyancy forcing by the atmospheric fluxes such as the latent heat loss due to monsoonal winds (McCreary and Kundu 1989; de Boyer Montégut et al. 2007). When looking deeper at the D25 variations (Figure 8b), there is a clear seasonal cycle both at the coast and offshore, with the seasonal upwelling signal (from June to October) radiating westward as a Rossby wave as has been abundantly described in literature (e.g. Shankar and Shetye 1997). Both the D25 and subtle seasonal ITLD variations are accurately captured by the model (Figures 7a and 8a). The model is in particular able to simulate the shoaling of the ITLD in summer along the western Indian coastline and the

contrasted ITLD behaviour from east to west. Table 2 further provides quantitative estimates of the mean offshore ITLD / D25 for model (14 m / 25 m) and observations (12 m / 21 m) during summer season, illustrating the realism of the model background state in this region.

In the western and northern Bay of Bengal, the observations display a similar ITLD evolution to the SEAS ITLD, with an annual periodicity close to the coast and a semi-annual periodicity away from the coast (Figure 7d and 7f). The maximum deepening of the offshore ITLD occurs in January, while a shallow ITLD is observed from April to October. Away from the coast, there is a secondary deepening developing during summer monsoon. The model captures the ITLD annual and semi annual periodicity respectively close to the coast and further offshore, with a slight underestimation of the offshore ITLD deepening during summer monsoon (Figure 7c and 7e). In the northernmost part of PK transect (Figure 7e), the modelled ITLD shows a very shallow offshore ITLD all year long. This area is not sampled by the observations, which typically do not exist shoreward of 21°N.

The D25 variations near the coast are also reasonably well reproduced by the model (Figure 8c-f). The summer mean values of the ITLD and D25 in the offshore BOB also agree quantitatively well (Table 2, 20 to 30 m for ITLD and ~70 m for D25). Unfortunately, no such repeated XBT transects have been performed in the STI region and quantitative validation of the model ITLD and D25 in this region is therefore not feasible.

4. Processes controlling the intraseasonal SST variability along the Indian coast

The agreement between the model and observed climatology (ITLD, D25) and intraseasonal forcing discussed in the previous section is reasonable enough to allow us investigating mechanisms of intraseasonal SST variations along the coasts of India with some confidence. The black curve in Figure 9 shows the typical time-evolution of an intraseasonal SST event in each region: the typical amplitude of intraseasonal SST variations is about 0.2°C for the three considered regions. Figures 9-13 show the typical variations of key-oceanic parameters (heat fluxes, wind stresses, MLD and D25) and time integrated heat budget terms associated with those SST variations, and allow understanding the key processes in each region.

Figure 10 shows the typical surface heat flux fluctuations associated with intraseasonal SST variations in each region. Intraseasonal net heat flux variations have typical amplitudes of ~20, ~10 and 22 W.m⁻² for the SEAS, STI and NWBoB regions, respectively. The amplitude and phase of the model intraseasonal net heat flux agree generally well with OAFlux and TropFlux (with 20-30% weaker heat flux fluctuations in the SEAS and STI in OAFlux). This analysis suggests that

shortwave fluctuations are the first contributor to the overall heat flux variability in these regions, shortwave contributing to as much as 75% in the SEAS region and to about 60% in the other regions. Latent heat flux perturbations explain most of the remaining variability.

Figure 9 displays the respective contribution of oceanic and atmospheric processes to intraseasonal SST in the three selected regions, while Table 3 summarizes these contributions. In all three regions, heat flux atmospheric forcing is the main contributor to SST variations (red curve on Figure 9; 109%, 72% and 171% of the SST variations in the SEAS, STI and NWBoB regions, respectively). The total contribution from oceanic processes however strongly varies from one region to another (plain blue curve on Figure 9). Oceanic processes only represent a weak negative contribution (-9%, Table 3) to the intraseasonal mixed layer heat budget in the SEAS region. They contribute to a larger extent to the SST variations in the STI and NWBoB where they contribute by 28% to (resp. reduce by 71%) SST intraseasonal variations. In the following, we will discuss more specifically each regions in order to understand their detailed mechanisms, and differences between regions.

Figure 11 allows explaining the marginal role of oceanic processes in the SEAS region. Intraseasonal SST fluctuations are associated with large wind stress perturbations of similar amplitude in the three selected regions (Figure 11). However, whereas most of this wind signal projects onto the along-shore component in the STI and NWBoB regions, most of the intraseasonal wind variations are in the same direction as the monsoon flow in the SEAS, that is broadly perpendicular to the west coast of India. The very weak along shore intraseasonal wind stress variations are hence unable to drive any significant intraseasonal fluctuations in the SEAS offshore upwelling. Intraseasonal Ekman pumping variations drive D25 intraseasonal variations in the SEAS (see the agreement between the time integral of Ekman pumping and D25 variations in Figure 12a), but these variations are small (typically less than 2m peak-to-through) and hence only marginally modulate oceanic processes at intraseasonal timescales (Figure 9a). The result is that intraseasonal SST fluctuations are essentially driven by surface heat flux perturbations in this region (see Table 3).

The picture is somewhat different for the STI region: there are larger along-shore wind stress and Ekman pumping perturbations (Figure 11b) and larger D25 intraseasonal variations (nearly 4m peak-to-trough, Figure 12b). Most of these D25 variations are associated with Ekman pumping in this region where only a small portion of coastline is present. This wind-driven Ekman divergence has two separate impacts: first, the D25 variations drive variations of vertical mixing (dashed line in Figure 9b). The deeper upper thermocline from days -15 to +15 (Figure 12b) reduces the cooling efficiency of the vertical mixing during this period. The integrated vertical mixing term is therefore

in phase quadrature with the SST and hence weakly contributes to SST intraseasonal fluctuations. Second, the wind-driven divergence / convergence of the surface circulation is associated with an intraseasonal modulation of the surface advection term (dash-dotted line in Figure 9b). The STI region does display a seasonal-average SST minimum, due to upwelling as shown in Rao et al. (2006; their figure 1). Surface divergence exports the coastal cold water into the whole STI box, hence contributing to a background cooling. Increased Ekman-induced downwelling signal from days -25 to 0 (Figure 12b) modulates this background cooling through intraseasonal fluctuations of the surface divergence, hence resulting in intraseasonal anomalies of the surface cooling (i.e. exporting more or less cold water from the coastal strip to the entire STI box). This process is the result of intraseasonal modulation of the coastal upwelling and is somewhat consistent with the studies of Rao et al. (2006) and Ganer et al. (2009). We however demonstrate more quantitatively than those two studies that surface heat flux forcing dominates the temperature changes, with secondary contributions (~30%) from intraseasonal modulation of the upwelling.

In the NWBoB, oceanic processes indeed strongly damp intraseasonal SST variations driven by intraseasonal surface heat fluxes perturbations (Table 3, Figure 9c). The oceanic contribution is largely driven by vertical mixing processes there, advective processes being very weak (Figure 9c). This surprising effect can neither be explained by upper thermocline fluctuations, which are very weak (Figure 12c) nor by wind amplitude fluctuations, which would rather act in phase with atmospheric forcing (Figure 11c). These intraseasonal variations of vertical mixing are related to intraseasonal changes of the stratification at the base of the thermocline (defined hereafter as the difference between the temperature at the base of the mixed layer minus the temperature 10m below). During a cooling event, the surface cools, while the subsurface temperature varies less, resulting in a decreased temperature gradient at the base of the mixed layer (Figure 13). This reduces the cooling efficiency of vertical mixing, i.e. results in a mixing-induced anomalous warming (Figure 9c) that opposes the surface heat fluxes-driven cooling tendency. Looking at the distribution of the actual cooling term (rather than at anomalies; not shown) reveals that, despite the presence of some barrier layer in the region (figure 6d), entrainment warming does not occur frequently: the entrainment intraseasonal contribution rather generally arises from a decrease of the background entrainment cooling. This mechanism is particularly efficient in the NWBoB region, for two reasons: first, the mean vertical temperature gradient during summer season (Table 4) is relatively weak ($\sim 0.2^{\circ}\text{C} / 10 \text{ m}$) compared to the SEAS ($\sim 0.4^{\circ}\text{C} / 10 \text{ m}$) and STI regions ($\sim 0.3^{\circ}\text{C} / 10 \text{ m}$); second, surface intraseasonal SST variations are larger here (Table 3) hereby enhancing the propensity of SST to modulate vertical gradient and mixing. As a result, intraseasonal fluctuations of this gradient

reach ~50% of the mean value in the NWBoB, while this intraseasonal modulation only reach 10 to 20% in the two other regions considered (Table 4).

The above results strongly suggest that atmospheric heat fluxes are the main contributor to intraseasonal SST fluctuations (~70 to 170 %) along the Indian coastline. The amplitude of the SST response to intraseasonal heat flux variations is however sensitive to MLD. We therefore assess the sensitivity of our results to the MLD product by calculating the surface heat flux-related SST intraseasonal variations using the simple slab ocean model defined by equation (2). We obtain SST fluctuations of similar amplitude to simulated ones in the SEAS and STI region, and a large overestimation in the NWBoB (Figure 14a) when integrating the model heat flux over the model MLD. Correlation between slab ocean model results and modelled intraseasonal SST variations exceeds 0.8 for both SEAS and NWBoB regions, whereas for the STI region it ranges between 0.5 and 0.6 due to the phase lag between oceanic and atmospheric contributions in this region (Figure 14c). These results suggest again that heat fluxes forcing dominate the SST signal (oceanic processes acting to damp the heat flux contribution in the NWBoB), in agreement with the mixed layer heat budget analysis in the model. Intraseasonal variations of the buoyancy forcing and frictional velocity act to modulate the MLD at intraseasonal timescales. As shown on Figure 12, these fluctuations reach 2 meters for typical events but can be as large as 5 meters for the strongest perturbations. The impact of these intraseasonal MLD fluctuations are thus investigated by comparing slab ocean model results using the actual model MLD and model climatological MLD. Not accounting for intraseasonal MLD fluctuations results in a 10% to 20% decrease of the SST amplitude, depending on the region (Figure 14a). This decrease can be explained in the following way: the MLD signal is roughly in phase opposition with the SST (Figure 12), with monsoon break phases being associated with both weak winds and positive buoyancy forcing anomalies. Taking into account MLD variations in equation 2 is hence going to decrease the effect of net heat flux forcing intraseasonal fluctuations. Using de Boyer Montégut et al. (2004) MLD climatology in place of the model one shows that the overestimation of the summer mixed layer depth along the coast in this dataset leads to a strong underestimation of the SST amplitude, ranging from 20-30% for the STI and SEAS regions to more than 50% in the NWBoB.

In contrast to the MLD dataset used, the amplitude of the SST perturbations appears to be less sensitive to the heat flux product used in the slab ocean model (Figure 14b). The model and TropFlux heat flux data results in very similar SST perturbations amplitude, while SST amplitude is slightly reduced by ~20% in the SEAS and STI region when using OAFflux.

5. Summary and discussion

a. Summary

In this paper, we have used an eddy permitting ($1/4^\circ$) regional ocean model in the Indian Ocean to investigate the main processes controlling intraseasonal SST variations along the coasts of India during boreal summer. Analysis of modelled and observed SST reveals that local intraseasonal SST variability maxima are found in three specific offshore regions: the south-eastern Arabian Sea (SEAS), the southern tip of India (STI) and the north-western part of the Bay of Bengal (NWBoB). The model intraseasonal heat flux and wind forcing as well as SST variability agrees well with observed estimates, although the model underestimates offshore SST fluctuations by about 20%. In addition, the model mixed layer and upper thermocline depth mean seasonal cycle are in good agreement with basin-scale climatologies and estimates derived from repeated XBT transects in the Indian offshore domain.

The model mixed layer heat budget analysis shows that intraseasonal SST variability along the Indian coastline is largely driven by atmospheric heat flux variations. Oceanic processes (advection and mixing) do however have contrasted contributions depending of the region. In the SEAS, contribution of oceanic processes is negligible as along-shore intraseasonal wind variations are very weak, preventing upwelling intraseasonal fluctuations. In the STI, both offshore upwelling and Ekman pumping drive vertical advection fluctuations that contribute to $\sim 30\%$ to the total SST fluctuations. Finally, in the NWBoB region, vertical mixing diminishes the effect of the atmospheric heat flux perturbations by 40%. These oceanic fluctuations are largely controlled by changes in the temperature gradient below the base of the mixed layer. When the mixed layer cools, the temperature difference with underlying water indeed diminishes, hence resulting in weaker (i.e. negative intraseasonal anomalies) vertical mixing.

Simple slab ocean model integrations show that the amplitude of intraseasonal mixed layer depth fluctuations enhances intraseasonal SST variations by 10% to 20%, the largest sensitivity being in the STI region. The gridded MLD product derived from Argo data (de Boyer Montégut et al. 2004) underestimates boreal summer MLD in Indian offshore regions due to a lack of observational coverage, resulting in a 20% underestimation of SST fluctuations in the SEAS and 60% underestimation in the NWBoB. In contrast, the amplitude of intraseasonal SST fluctuations is not very sensitive to the heat flux dataset, with TropFlux and OAFlux datasets giving similar results to our model.

b. Discussion

There have been several studies that diagnosed processes responsible for SST intraseasonal variations during summer over the Bay of Bengal. Vialard et al. (2012) suggest that air-sea fluxes are responsible of ~90% of the SST variations over the Bay of Bengal, and that this number does not vary strongly from year to year. While observational studies generally do not quantify exactly the contribution of fluxes against other processes, most of them attributed a large part of the SST large-scale variations in the Northern Bay of Bengal to intraseasonal air-sea fluxes (e.g. Sengupta and Ravichandran 2001; Duvel and Vialard 2007). The Duncan and Han (2009) model study also suggests that air-sea fluxes (and more specifically latent heat flux variations) dominate SST variability in the Bay of Bengal, but the region they selected is not in the area of the maximum SST intraseasonal variability. The Vinayachandran et al. (2012) study show that air-sea fluxes dominate intraseasonal SST variations in the northern Bay of Bengal. Several other modelling studies (Fu et al. 2003; Waliser et al. 2004; Bellon et al. 2008), suggest that air-sea flux is the dominant process that drives intraseasonal variability in the Northern Bay of Bengal; however, they also find a non-negligible contribution of oceanic processes (mixing, Ekman pumping, vertical advection). We find that oceanic processes diminish by ~40% the SST variations driven by surface fluxes, i.e. a significant negative feedback. This is a larger contribution than in previous studies, but our study specifically focuses on the offshore region, and the contribution of oceanic processes diminishes when a larger box is selected or when the box is shifted away from the offshore region.

Two recent studies by Rao et al. (2011) and Vinayachandran et al. (2012) suggested that the salinity structure matters for intraseasonal SST variations in the north-western Bay of Bengal. Rao et al. (2011) suggest that intraseasonal variations of the SSS and SST may be driven by intraseasonal variations of the river discharge, through modulation of the mixed layer depth. We find that intraseasonal variations of the MLD increase the intraseasonal SST variations amplitude by up to 20%, suggesting that intraseasonal variations of MLD (and SSS), although non-negligible, do not play a primary role. Vinayachandran et al. (2012) rather emphasize the effect of the mean salinity structure, with lower sensitivity as the result of enhanced river runoff. Their sensitivity experiment (observed runoff multiplied by 10) however seems pushed to the far side of river runoff uncertainties. Our results showing that the amplitude of the SST intraseasonal signal is sensitive to the MLD is however in agreement with their statement that the mean salinity structure can have a large influence on the SST intraseasonal variability. Although we do not quantify the salinity effects in the current study, we agree that the background salinity structure is probably important for simulating the background mixed layer depth and intraseasonal SST variations in the north-western

Bay of Bengal. Our detailed validation to basin-scale climatologies and offshore upper ocean thermal structure however suggests that our model has a reasonable climatological seasonal cycle of upper ocean haline and thermal state, hence lending some confidence to the quantitative estimates in our study.

There are to our knowledge no other detailed studies of the processes of intraseasonal SST variations in the SEAS region. In the STI region, Rao et al. (2006) find that intraseasonal heat fluxes play a negligible role, with wind-stress induced oceanic response explaining most of the intraseasonal SST response. The analysis of Rao et al. (2006) however focuses on analyses at a single ocean point (78°E and 7.5°N). At this location, our model displays a larger contribution of oceanic vertical processes (60%) compared to the box average (30%), somewhat consistently with the results of Rao et al. (2006). The modelling studies of Vialard et al. (2012) and Ganer et al. (2009) also suggest a larger role of vertical oceanic processes, while our results put more emphasis on air-sea fluxes and less (~30%) on contributions from the upwelling. Vialard et al. (2012) used a similar strategy to the present paper, although with a different ocean model, and with lower resolution (1° against ¼° here), while Ganer et al. (2009) used a much simpler model. It is thus hard to tell which of the two hypotheses (dominating effect of heat fluxes or of upwelling) is correct. Future studies are probably needed in order to provide more clues as whether atmospheric heat flux forcing plays a role in this region.

In this paper, we described the “average” contribution of each processes to intraseasonal variations of SST. Figure 15 shows the contributions of various processes to intraseasonal SST variations for the summer of 2000 (i.e. the intraseasonal events discussed by Vecchi and Harrison 2002). The dominating term in all regions is atmospheric forcing, in agreement with the average picture from Table 3. But oceanic contributions are sometimes quite different from the average picture, like for example in the STI or for the first cooling event in the SEAS, where vertical oceanic processes fight atmospheric forcing, unlike in the mean picture where they do not clearly contribute. The average picture that we give should hence not obscure the fact that there are significant event-to-event fluctuations, and that our description may not agree with individual case studies (like, e.g. Rao et al. 2006).

In this paper, we have focussed on the thermodynamical response of the Northern Indian Ocean to the boreal summer intraseasonal variability. But Vialard et al. (2009) did show that there is additionally a dynamical response. The basin scale intraseasonal wave propagations discussed by Vialard et al. (2009) from observations are remarkably well reproduced by the model (not shown). Equatorial wind fluctuations associated with active-break phases of the monsoon force equatorial

Kelvin waves that eventually propagate along the rim of the Bay of Bengal as coastally trapped Kelvin waves, hence modulating the sea level and thermocline variability there. These waves occur with a stable phase relation with the SST signals (due to the common atmospheric forcing: monsoon active and break phases), and hence do result in intraseasonal variations of the thermocline depth in the three boxes, with some time offset with the local forcing. These wave propagations however do not influence SST because of the weak influence of mixing and upwelling (the two physical processes that could be modulated by those waves) in most regions, as demonstrated by the current study.

There are of course limitations to the current study. We showed that uncertainties in the mixed layer depth can have a large effect on the estimate of the role of air-sea fluxes. The thermocline depth and salinity structure may also play a strong role by affecting the magnitude of entrainment cooling from the subsurface (e.g., Vinayachandran et al. 2012). We also focus on the coastal and offshore (??) region where there is only a limited coverage of validation data. While our model displays some noticeable differences with large-scale products (see figure 6), they are not larger than any other state-of-the-art simulation in the region with a similar horizontal resolution (e.g. Vinayachandran et al. 2012). In addition, the model has been specifically validated in the coastal region with ship-of-opportunity XBT data. The model has a good performance in reproducing the observed background seasonal cycle of the isothermal layer and thermocline depth close to the coast (figures 7 and 8), and reproduces quite well intraseasonal oscillations in those coastal regions (figure 3), despite some underestimation, which could however be linked to the tendency of TMI SST to overestimate intraseasonal variability (Bhat et al. 2004). Our model hence seems in reasonable agreement with available data. A more careful validation of models is however probably needed in the offshore regions of the Bay of Bengal.

The current study focuses quite specifically on coastal and offshore regions, for which data coverage is sparse, and sometimes in disagreement with basin-scale products. We have for example no direct MLD observations in the STI region. One can also have doubts about the quality of air-sea fluxes close to the coast, where inflow of dry land air and sea-breeze effects may not be well resolved. There is hence probably a need for specific offshore observation networks, in addition to existing-basin scale observations, in order to support studies in offshore regions better.

Acknowledgements: We thank the Ministry of Earth Sciences, Government of India for the support through INCOIS, Hyderabad for conducting systematic XBT surveys. JV and ML are funded by Institut de Recherche pour le Développement (IRD) and did part of this work while visiting National Institute of Oceanography (NIO, India). KN acknowledges the financial support from the Council of Scientific and Industrial Research, India. This work was performed using HPC resources from GENCI-IDRIS (Grant 2009- 011140). This is NIO contribution number xxxx.

References:

- Bailey R, Gronell A, Philips H, Tanner E, Meyers G (1994) Quality Control Cook Book for XBT Data. Report 221. CSIRO, Marine Laboratories.
- Barnier B, et al. (2006) Impact of partial steps and momentum advection schemes in a global ocean circulation model at eddy permitting resolution. *Ocean Dyn.* 56: 543-567, doi:10.1007/s10236-006-0082-1.
- Bellon G, Sobel AH, Vialard J (2008) Ocean-atmosphere coupling in the monsoon intraseasonal oscillation: a simple model study. *J. Clim.* 21: 5254-5270.
- Bhat GS, Vecchi GA, Gadgil S (2004) Sea surface temperature of the Bay of Bengal derived from TRMM Microwave Imager. *J. Atmos. Oceanic Technol.* 21, 1283-1290.
- Blanke B, Delecluse P (1993) Variability of the tropical Atlantic ocean simulated by a general circulation model with two different mixed layer physics. *J. Phys. Oceanogr.* 23: 1363-1388. doi: 10.1175/1520-0485(1993)023<1363:VOTTAO>2.0.CO;2.
- Brodeau L, Barnier B, Treguier A-M, Penduff T, Gulev S (2010) An ERA40-based atmospheric forcing for global ocean circulation models. *Ocean Modell.* 3: 88-104, doi:10.1016/j.ocemod.2009.10.005.
- Chatterjee P, Goswami BN (2004) Structure, genesis and scale selection of the tropical quasi-biweekly mode. *Q. J. R. Meteor. Soc.* 130: 1171-1194.
- Chatterjee A, Shankar D, Shenoi SSC, Reddy GV, Michael GS, Ravichandran M, Gopalkrishna VV, Rama Rao EP, Udaya Bhaskar TVS, Sanjeevan VN (2012) A new atlas of temperature and salinity for the North Indian Ocean. *J. Earth Syst. Sci.* 121: 559-595.
- Dai A, Trenberth KE (2002) Estimates of freshwater discharge from continents: Latitudinal and seasonal variations. *J. Hydrometeor.* 3: 660-687.
- de Boyer Montegut C, Madec G, Fischer AS, Lazar A, Iudicone D (2004) Mixed layer depth over the global ocean: an examination of profile data and a profile-based climatology. *J. Geophys. Res.* 109: C12003. doi:10.1029/2004JC002378.
- de Boyer Montegut C, Vialard J, Shenoi SSC, Shankar D, Durand F, Ethe C, Madec G (2007) Simulated seasonal and interannual variability of mixed layer heat budget in the northern Indian Ocean. *J. Clim.* 20: 3249-3268.
- Dee DP, Uppala S (2009) Variational bias correction of satellite radiance data in the ERA-Interim reanalysis. *Q. J. R. Meteorol. Soc.* 135: 1830-1841.
- Drakkar Group (2007) Eddy-permitting Ocean circulation hindcasts of past decades. *Clivar Exchanges* No 42, 12(3), 8-10.

- Duncan B, Han W (2009) Indian Ocean intraseasonal sea surface temperature variability during boreal summer: Madden-Julian Oscillations versus submonthly forcing and processes. *J. Geophys. Res.* 114: C05002. doi 10.1029/2008JC004958.
- Dussin R, Treguier A-M, Molines JM, Barnier B, Penduff T, Brodeau L, Madec G (2009) Definition of the interannual experiment ORCA025-B83, 1958-2007. LPO Report 902.
- Duvel JP, Vialard J (2007) Indo-Pacific sea surface temperature perturbations associated with intraseasonal oscillations of the tropical convection. *J. Clim.* 20: 3056-3082.
- Fu X, Wang B, Li T, McCreary JP (2003) Coupling between northward propagating, intraseasonal oscillations and sea-surface temperature in the Indian Ocean. *J. Atmos. Sci.* 60: 1733-1783.
- Gadgil S, Joseph PV, Joshi NV (1984) Ocean-atmosphere coupling over monsoon regions. *Nature* 312:141-145.
- Ganer DW, Deo AA, Gnanaseelan C (2009) Variability of mini cold pool off the southern tip of India as revealed from a thermodynamic upper ocean model. *Meteorol. Atmos. Phys.* 104: 229-238.
- Gopalakrishna VV, Durand F, Nisha K, Lengaigne M, Costa J, Rao RR, Ravichandran M, Amritash S, John L, Girish K, Ravichandran C, Suneel V (2010) Observed intra-seasonal to interannual variability of the upper ocean thermal structure in the South-Eastern Arabian Sea during 2002-2008. *Deep Sea Res.* 57: 739-754.
- Goswami BN (2005) South Asian Monsoon. In: Lau WKM, Waliser DE (eds) *Intraseasonal variability in the atmosphere-ocean climate system*. Praxis Springer, Berlin, pp 19-55.
- Goswami BN, Ajaya Mohan RS (2001) Intraseasonal oscillations and interannual variability of the Indian summer monsoon. *J. Clim.* 14: 1180-1198.
- Griffies SM, Biastoch A, Böning CW, Bryan F, Chassignet E, England M, Gerdes R, Haak H, Hallberg EW, Hazeleger W, Jungclaus J, Large WG, Madec G, Samuels BL, Scheinert M, Gupta AS, Severijns CA, Simmons HL, Treguier A-M, Winton M, Yeager S, Yin J (2009) Coordinated ocean-ice reference experiments (COREs). *Ocean Modell.* 26: 1-46. doi:10.1016/j.ocemod.2008.08.007.
- Huffman GJ, Adler RF, Arkin P, Chang A, Ferraro R, Gruber A, Janowiak J, McNab A, Rudolf B, Schneider U (1997) The Global Precipitation Climatology Project (GPCP) Combined Precipitation Dataset. *Bull. Amer. Meteor. Soc.* 78, 5-20.
- Joseph PV, Sabin TP (2008) An ocean-atmosphere interaction mechanism for the active break cycle of the Asian summer monsoon. *Clim. Dyn.* 30: 553-566.
- Joseph PV, Sijikumar S (2004) Intraseasonal variability of the low level jet stream of the Asian summer monsoon. *J. Clim.* 17: 1449-1458.
- Keerthi MG, Lengaigne M, Vialard J, de Boyer Montégut C, Muraleedharan PM (2012) Interannual variability of the Tropical Indian Ocean mixed layer depth, *Clim. Dyn.* accepted.
- Large WG, Yeager SG (2004) Diurnal to decadal global forcing for ocean and sea-ice models: the data sets and flux climatologies. NCAR/TN-460 STR, 111 pp.
- Lawrence DM, Webster PJ (2002) The boreal summer intraseasonal oscillation: relationship between eastward and northward movement of convection. *J. Atmos. Sci.* 59: 1593-1606.
- Le Sommer J, Penduff T, Theetten S, Madec G, Barnier B (2009) How momentum advection schemes influence current-topography interactions at eddy-permitting resolution. *Ocean Modell.* 29: 1-14. doi:10.1016/j.ocemod.2008.11.007.

- Lengaigne M, Hausmann U, Madec G, Menkes C, Vialard J, Molines JM (2012) Mechanisms controlling warm water volume interannual variations in the equatorial Pacific: diabatic versus adiabatic processes. *Clim. Dyn.* 38(5-6): 1031-1046. doi 10.1007/s00382-011-1051-z.
- Locarnini RA, Mishonov AV, Antonov JI, Boyer TP, Garcia HE, Baranova OK, Zweng MM, Johnson DR (2010) *World Ocean Atlas, 2009, vol 1: Temperature*. S. Levitus (ed) NOAA Atlas NESDIS 68. U.S. Government Printing Office, Washington, D.C.
- Madec G (2008) "NEMO ocean engine". Note du Pole de modélisation, Institut Pierre-Simon Laplace (IPSL), France, No 27 ISSN No 1288-1619.
- Maneesha K, Sarma VVSS, Reddy NPC, Sudhram Y, Ramana Murty TV, Sarma VV, Kumar D (2010) Meso-scale atmospheric events promote phytoplankton blooms in the coastal Bay of Bengal. *J. Earth Syst. Sci.* 120: 773-782.
- McCreary JP, Kundu PK (1989) A numerical investigation of sea surface temperature variability in the Arabian Sea. *J. Geophys. Res.* 94(C11): 16,097-16,114.
- Nidheesh AG, Lengaigne M, Vialard J, Unnikrishnan AS, Dayan H (2012) Decadal sea level variability in the tropical Indo Pacific: results from an ocean model and the CMIP3 database. *Clim. Dyn.* submitted.
- Penduff T, Le Sommer J, Barnier M, Treguier A-M, Molines JM, Madec G (2007) Influence of numerical schemes on current-topography interactions in $\frac{1}{4}^\circ$ global ocean simulations. *Ocean Sci.* 3: 509-524.
- Prasad TG (2004) A comparison of mixed-layer dynamics between the Arabian Sea and Bay of Bengal: One-dimensional model results. *J. Geophys. Res.* 109, C03035. doi 10.1029/2003JC002000.
- Praveen Kumar B, Vialard J, Lengaigne M, Murty VSN, McPhaden MJ (2010) Tropflux: air-sea fluxes for the global tropical oceans-description and evaluation against observations. *Clim. Dyn.* doi: 10.1007/s00382-011-1115-0.
- Praveen Kumar B, Vialard J, Lengaigne M, Murty VSN, McPhaden MJ, Cronin M, Gopala Reddy K (2012) TropFlux Surface wind stress over the tropical oceans: Comparison and evaluation. *Clim. Dyn.* submitted.
- Rao RR, Girish Kumar MS, Ravichandran M, Samala BK, Anitha G (2006) Observed intraseasonal variability of mini-cold pool off the southern tip of India and its intrusion into the south central Bay of Bengal during summer monsoon season. *Geophys. Res. Lett.* 33: L15606. doi:10.1029/2006GL026086.
- Rao SA, et al. (2011) Modulation of SST, SSS over northern Bay of Bengal on ISO time scale. *J. Geophys. Res.* 116: C09026. doi:10.1029/2010JC006804.
- Roxy M, Tanimoto Y (2007) Role of SST over the Indian ocean in influencing intraseasonal variability of the Indian summer monsoon. *J. Met. Soc. Jpn.* 85: 349-358.
- Sengupta D, Goswami BN, Senan R (2001) Coherent intraseasonal oscillations of ocean and atmosphere during the Asian summer monsoon. *Geophys. Res. Lett.* 28: 4127-4130. doi:10/1029/2001GL013587.
- Sengupta D, Ravichandran M (2001) Oscillations of Bay of Bengal sea surface temperature during the 1998 summer monsoon. *Geophys. Res. Lett.* 28: 2033-2036.
- Shankar D, and Shetye SR (1997) On the dynamics of the Lakshadweep high and low in the southeastern Arabian Sea. *J. Geophys. Res.* 102: 12551-12562.

- Shenoi SSC, Shankar D, Shetye SR, (2002) Differences in heat budgets of the near-surface Arabian Sea and Bay of Bengal: Implications for the summer monsoon. *J. Geophys. Res.* 107: 3052. doi:10.1029/2000JC000679.
- Thadathil P, Prasad T, Rao RR, Muraleedharan PM, Somayajulu YK, Gopalakrishna VV, Murtugudde R, Reddy GV, Revichandran C (2008) Seasonal variability of the observed barrier layer in the Arabian Sea. *J. Phys. Oceanogr.* 38: 624-638.
- Treguier A-M, Barnier B, De Miranda AP, Molines JM, Grima N, Imbard M, Madec G, Messenger C, Reynaud T, Michel S (2001) An eddy-permitting model of the Atlantic circulation: Evaluating open boundary conditions. *J. Geophys. Res.* 106: 22,115-22,129.
- Uppala SM, et al. (2005) The ERA-40 re-analysis. *Q. J. R. Meteorol. Soc.* 131: 2961-3012.
- Vecchi GA, Harrison DE (2002) Monsoon breaks and subseasonal sea surface temperature variability in the Bay of Bengal. *J. Clim.* 15: 1485-1493.
- Vialard J, Shenoi SSC, McCreary JP, Shankar D, Durand F, Fernando V, Shetye SR (2009) Intraseasonal response of Northern Indian Ocean coastal waveguide to the Madden-Julian Oscillation. *Geophys. Res. Lett.* 36: L14605. doi:10.1029/2008GL037010.
- Vialard J, Jayakumar A, Gnanaseelan C, Lengaigne M, Sengupta D, Goswami BN (2012) Processes of 30-90 day sea surface temperature variability in the Northern Indian Ocean during boreal summer. *Clim. Dyn.* doi: 10.1007/s00382-011-1015-3.
- Vinayachandran PN, Neema CP, Mathew S, Remya R (2012) Mechanisms of summer intraseasonal sea surface temperature oscillations in the Bay of Bengal, *J. Geophys. Res.* 117: C01005. doi:10.1029/2011JC007433.
- Vinayachandran PN, Yamagata T (1998) Monsoon response of the sea around Sri Lanka: generation of thermal domes and anticyclonic vortices. *J. Phys. Oceanogr.* 28: 1946-1950.
- Vinayachandran PN, Mathew S (2003) Phytoplankton bloom in the Bay of Bengal during the northeast monsoon and its intensification by cyclones. *Geophys. Res. Lett.* 30(11), 1572, doi:10.1029/2002GL016717.
- Waliser DE, Murtugudde R, Lucas LE (2004) Indo-Pacific Ocean response to atmospheric intraseasonal variability: 2. Boreal summer and the intraseasonal oscillation. *J. Geophys. Res.* 109: C03030. doi: 10.1029/ 2003JC002002.
- Webster PJ, Magana VO, Palmer TN, Shukla J, Tomas RA, Yanai M, Yasunari T (1998) Monsoons: processes, predictability, and the prospects for prediction. *J. Geophys. Res.* 103: 14451-14510.
- Wentz FJ, Gentemann C, Smith D, Chelton D (2000) Satellite measurements of sea-surface temperature through clouds. *Science* 288: 847-850.
- Xie P, Arkin PA (1997) Global Precipitation: A 17-year monthly analysis based on gauge observations, satellite estimates, and numerical model outputs. *Bull. Am. Meteor. Soc.* 78: 2539-2558.
- Yu L, Weller RA (2007) Objectively analyzed air-sea heat fluxes (OAFlux) for the global oceans. *Bull. Am. Meteor. Soc.* 88: 527-539.
- Zhang Y, Rossow WB, Lacis AA, Oinas V, Mishchenko MI (2004) Calculation of radiative fluxes from the surface to top of atmosphere based on ISCCP and other global data sets: Refinements of the radiative transfer model and the input data. *J. Geophys. Res.* 109. doi: 10.1029/2003JD004457.

Table captions:

Table 1: Validation of the modeled net heat flux variability in the three regions investigated in this study (SEAS, STI, NWBoB). The third line gives the standard deviation of the box-averaged 30-110d filtered net heat flux from model output, TropFlux (TF) and OAFlux (OA) datasets. The fourth line gives the correlation of the box-averaged 30-110d filtered net heat flux correlation of the model with TropFlux and OAFlux.

Table 2: Climatological MLD and D25 during summer season (JJAS) for model and XBT observations in the offshore regions of the PK (Port Blair-Kolkata), CP (Chennai-Port Blair) and KL (Kochi-Ladaksweep) transects (see figure 4a for locations).

Table 3: First line: standard deviation of the model 30-110 day filtered average SST in the three selected regions in this paper. Following lines: regression coefficients of time integrated 30-110 day filtered intraseasonal tendency terms to 30-110 day filtered SST fluctuations in the same regions. By construction, the second and third lines add up to 100%, and the last 2 lines show the decomposition of oceanic processes into lateral advection and vertical mixing. Only values significant at 99% are shown. Insignificant regression coefficients are indicated by NA.

Table 4: First line: Climatological temperature change at the bottom of the mixed layer (mixed layer temperature minus temperature 10 m below the mixed layer base, °C) during summer season (JJAS) for the model in the three selected regions. Second line: standard deviation of the 30-110 day filtered temperature change at the bottom of the mixed layer during summer season (JJAS) for the model in the three selected regions.

Figures captions:

Figure 1: June–September standard deviation of 1998–2007 30–110 day bandpass filtered SST for (a) TMI observations and (b) model. Units are in °C. The red boxes indicate the various regions along the coast of India selected in this paper: SEAS (73°E–77°E, 9°N–12°N), STI (74°E–78°E, 5°N–9°N) and NWBoB (80°E–85°E, 15°N–19°N).

Figure 2: June–September standard deviation of 1998–2007 30–110 day bandpass-filtered net surface heat fluxes ($\text{W}\cdot\text{m}^{-2}$) from (a) Tropflux dataset and (b) model; wind stress modulus (in $\text{N}\cdot\text{m}^{-2}$) from (c) TropFlux stress dataset and (d) model (see text for details).

Figure 3: Average 30–110 days bandpass filtered SST for TMI (red) and the model (black) for the three regions displayed in Fig. 1: (a) SEAS, (b) STI and (c) NWBoB. The correlation coefficient and the standard deviation ratio of model against observations for the JJAS period are indicated in each panel. The JJAS period is highlighted by a grey shading.

Units are in °C.

Figure 4: June–September climatological values of the 25°C isotherm depth from (a) the WOA09 database (Locarnini et al. 2009) and (b) the model. The black lines on panel (a) indicate the XBT transect used for validation purposes: Kochi-Lakshawep (KL, 72°E–76°E, 10°N–11°N), Port Blair-Kolkata (PK, 93°E–88°E, 11.5°N–21°N) and Chennai-Port Blair (CP, 82°E–92°E, 11°N–12°N). The red boxes on panel (b) indicates the various regions along the coast of India selected in this paper: SEAS (73°E–77°E, 9°N–12°N), STI (74°E–78°E, 5°N–9°N) and NWBoB (80°E–85°E, 15°N–19°N). Units are in m.

Figure 5: June–September climatological values of the mixed layer depth based on a density criterion from (a) de Boyer Montégut et al. (2004) and (b) the model. (c) Number of individual profiles per month and per $2\times 2^\circ$ box used to calculate de Boyer Montégut et al. (2004) MLD climatology. The black lines indicate on panel (a) the XBT transect used for validation purposes: Kochi-Lakshawep (KL, 72°E–76°E, 10°N–11°N), Port Blair-Kolkata (PK, 93°E–88°E, 11.5°N–21°N) and Chennai-Port Blair (CP, 82°E–92°E, 11°N–12°N). The red boxes on panel (b) indicate the various regions along the coast of India selected in this paper: South-Eastern Arabian Sea (SEAS, 73°E–77°E, 9°N–12°N), Southern Tip of India (STI, 74°E–78°E, 5°N–9°N) and North-Western Bay of Bengal (NWBoB, 80°E–85°E, 15°N–19°N). Units are in m.

Figure 6: June-September climatological values of the sea surface salinity (panels a and b, psu) and barrier layer thickness (panels c and d, m) for observations and the model. Barrier layer thickness observations are from the de Boyer Montegut et al. (2004) climatology. SSS observations are from the Chatterjee et al. (2012) climatology.

Figure 7: Seasonal cycle of the isothermal layer depth, computed from a temperature criterion (SST-0.2°C) for the model (left column) and XBT data (right column) along the XBT transects displayed on Figure 5a: SEAS (KL: Kochi-Ladakh sweep, top panel), western Bay of Bengal (CP: Chennai-Port Blair, middle panel) and northern Bay of Bengal (PK: Port Blair-Kolkata, bottom panel). Units are in m.

Figure 8: Seasonal cycle of the depth of the 25°C isotherm for the model (left column) and XBT data (right column) along the XBT transects displayed on Figure 5a: SEAS (KL: Kochi-Ladakh sweep, top panel), western Bay of Bengal (CP: Chennai-Port Blair, middle panel) and northern Bay of Bengal (PK: Port Blair-Kolkata, bottom panel). Units are in m.

Figure 9: June-September lag-regression coefficients of each process contributing to the 30-110 day filtered mixed layer heat budget to the normalized 30-110 day filtered SST in the 3 selected boxes shown in figure 5b. This figure hence shows the typical time-evolution of SST (black curve) for an intraseasonal SST event in the three boxes, and contributions from various processes. Units are in °C.

Fig 10: 30-110 day bandpass filtered net heat flux and related components regressed to the normalized average 30-110 day bandpass filtered SST in JJAS, averaged over the SEAS, STI and NWBoB regions. Units are in $W.m^{-2}$.

Figure 11: June-September lag-regression coefficients of the 30-110 day filtered model wind stress modulus, along shore (positive when conducive to offshore upwelling) and cross shore (positive inland) components to the normalized 30-110 day filtered SST in the 3 boxes shown in figure 5b. Units are in $N.m^{-2}$.

Figure 12: June-September lag-regression coefficients of the 30-110 day filtered model D25 (black curve), MLD (red curve) and time-integrated Ekman pumping (blue curve) to the normalized 30-110

day filtered SST in the 3 boxes shown in Figure 5b. Units are in m.

Figure 13: Lag-regression coefficients of Tdiff against total SST evolution at intraseasonal time scales for the NWBoB box. Tdiff is calculated as the difference between the temperature at the base of the mixed layer minus the temperature 10m below. Units are in °C.

Figure 14: Bar diagrams showing the standard deviation ratio of SST intraseasonal variations calculated from a slab ocean model using (a) different MLD estimates (model MLD, climatological model MLD and de Boyer Montegut et al. (2004) MLD) and (b) different heat flux estimates (Model fluxes, TropFlux product, OAFflux product) to modeled intraseasonal SST. (c-d) Same as (a-b) but for correlation. Model heat fluxes are used in panels (a-c). Model MLD is used in panels (b-d).

Figure 15: Time series of the 30-110d integrated tendency terms and SST evolution for summer 2000.

Table 1:

Dataset	SEAS			STI			NWBoB		
	Model	TF	OA	Model	TF	OA	Model	TF	OA
STD(Net)	28.58	27.63	21.68	24.58	24.29	18.81	33.68	35.18	34.05
Cor	NA	0.88	0.86	NA	0.85	0.79	NA	0.92	0.93

Table 2:

Region		Model	XBT
Kolkatta	MLD	22	19
	D25	71	66
Chennai	MLD	31	34
	D25	72	75
Kochi	MLD	14	12
	D25	25	21

Table 3:

	SEAS	STI	NWBoB
STD (°C)	0.19	0.16	0.22
Atm. processes	109 %	72 %	171 %
Oceanic processes	- 9 %	28 %	-71 %
Lateral advection	NA	31 %	NA
Vertical mixing	-12 %	NA	-72 %

Table 4:

	SEAS	STI	NWBoB
Mean TDiff	0.42	0.33	0.18
STD TDiff	0.10	0.08	0.10

Figure 1:

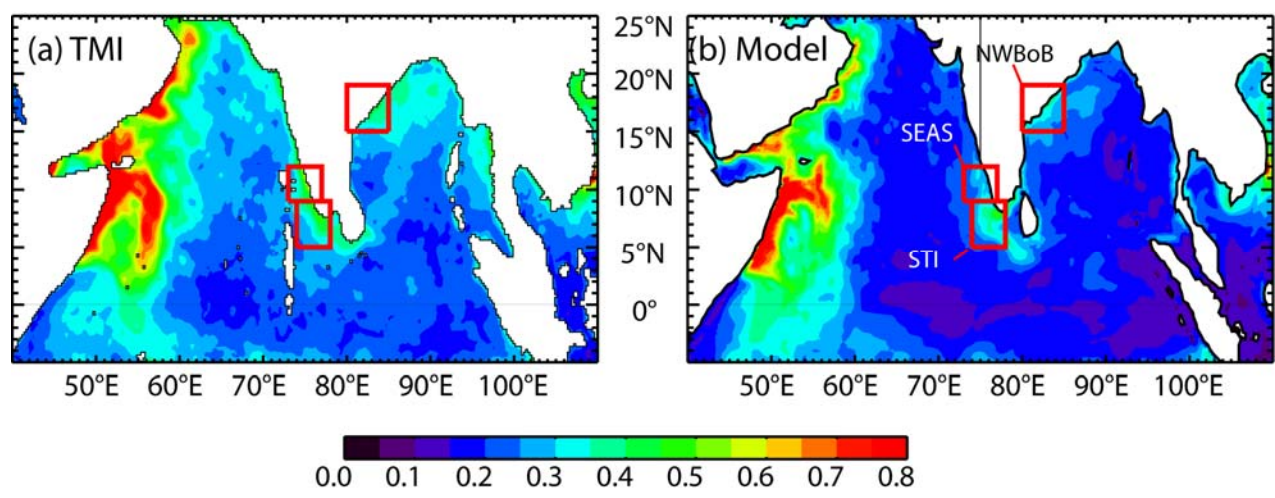


Figure 2:

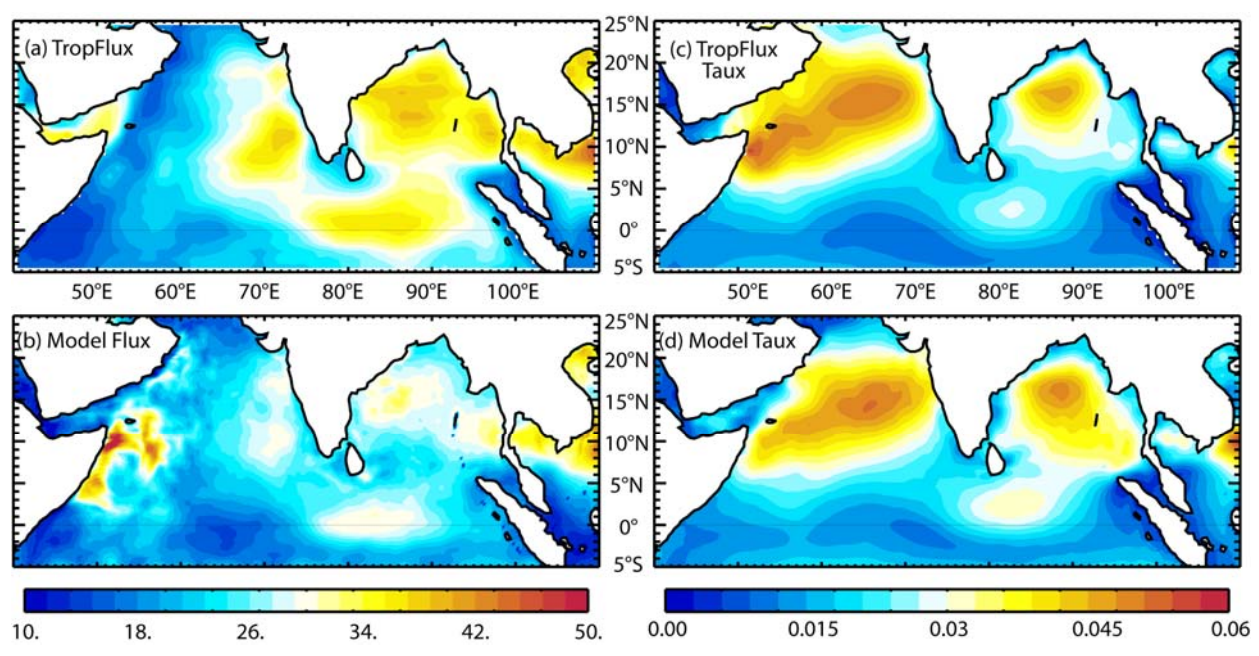


Figure 3:

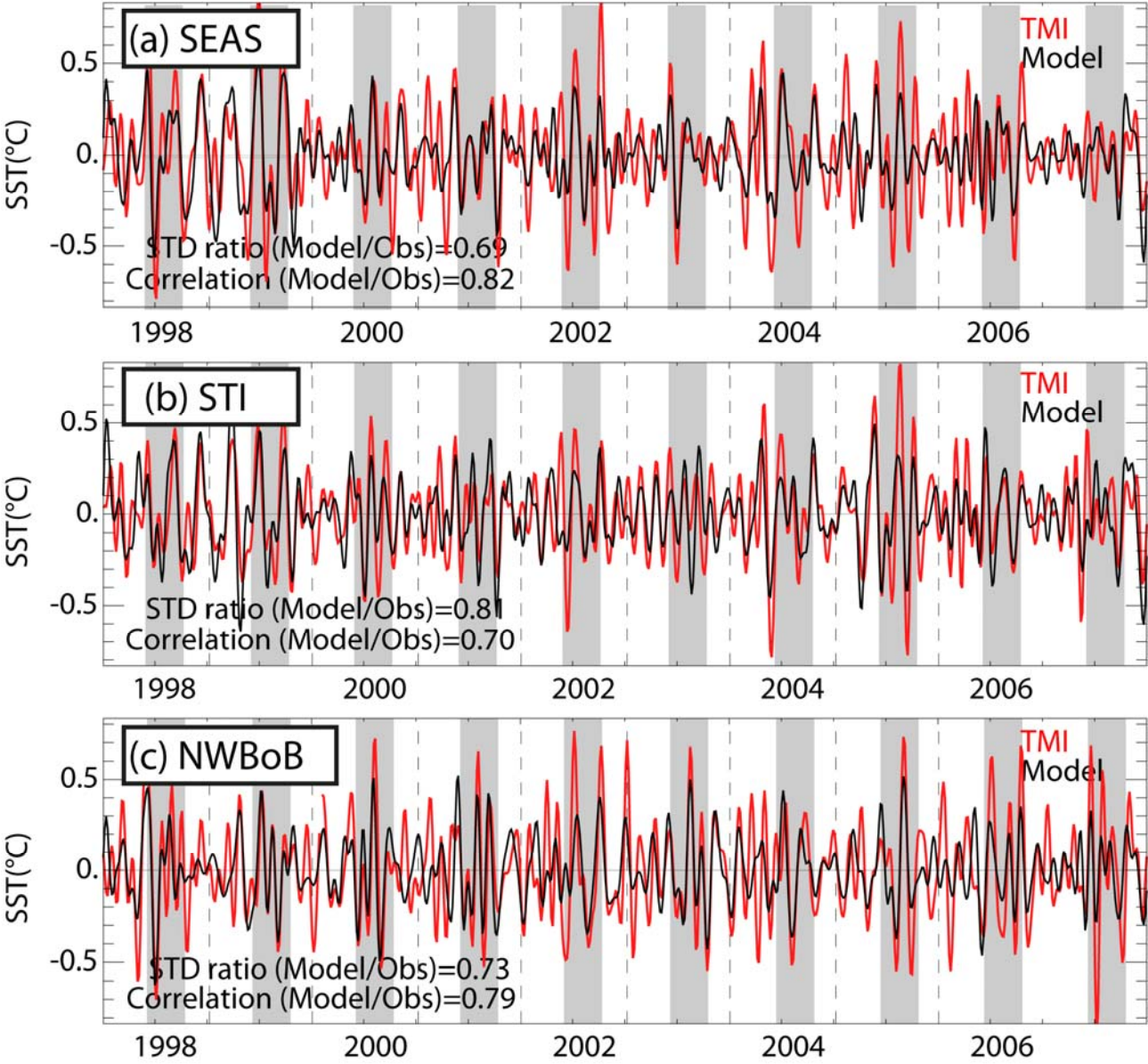


Figure 4:

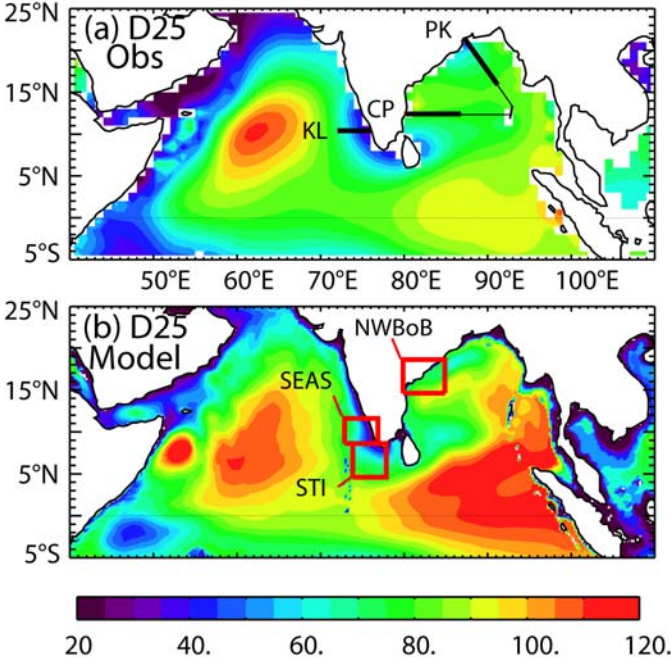


Figure 5:

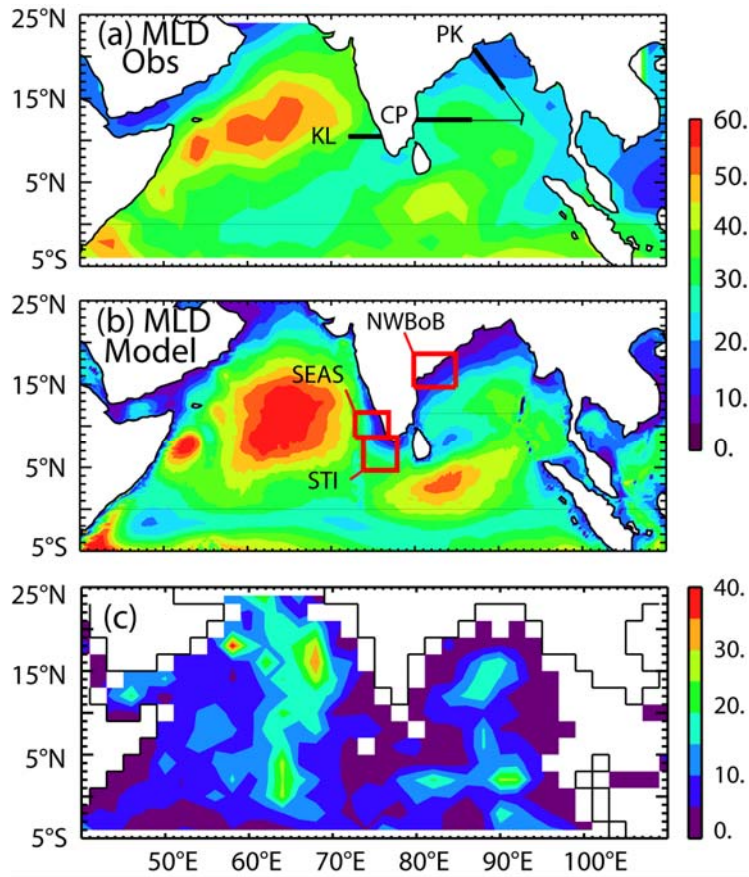


Figure 6:

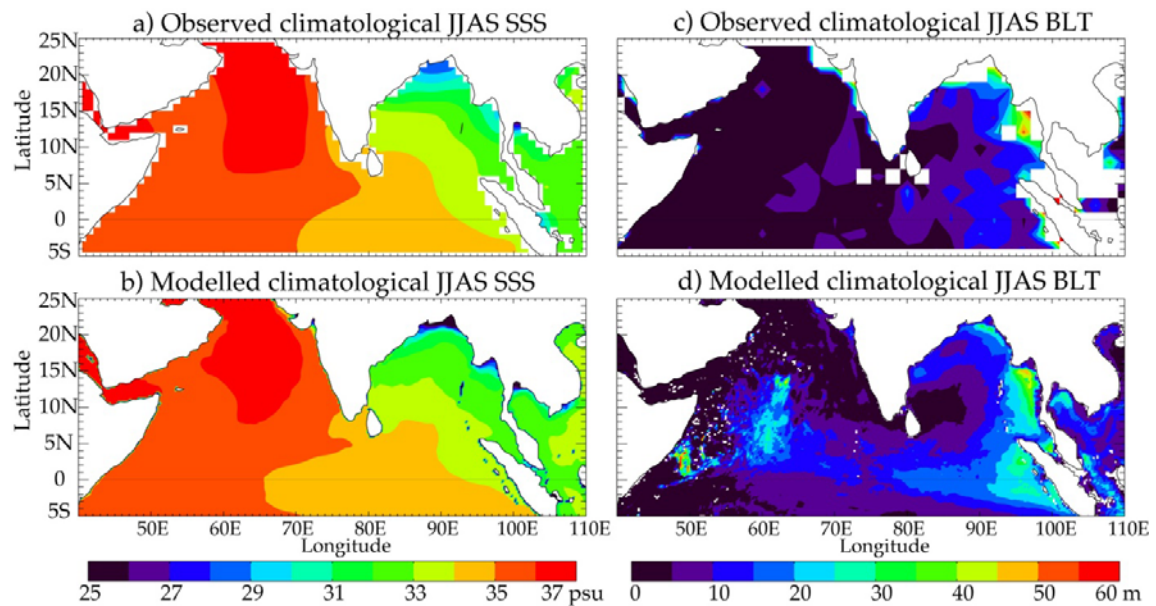


Figure 7:

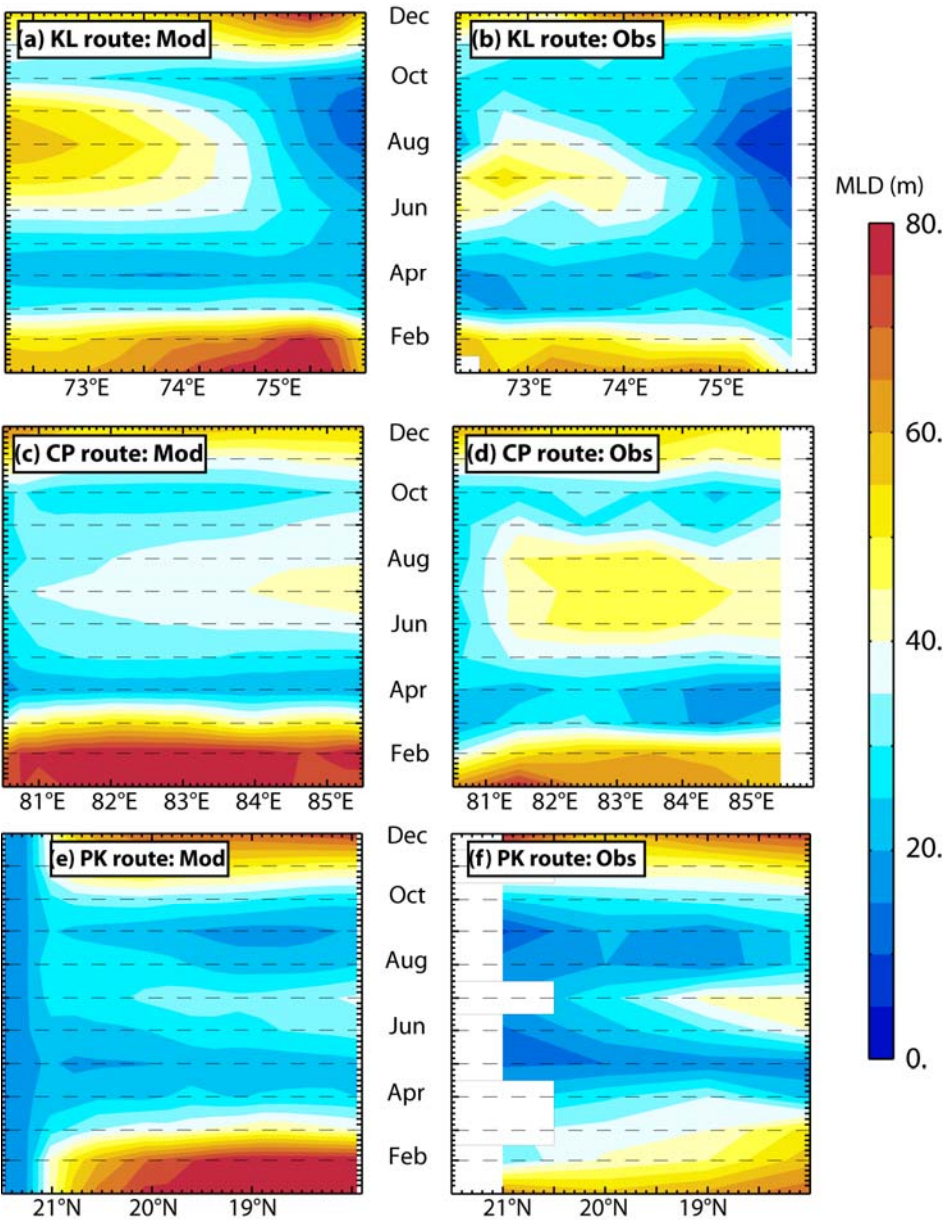


Figure 8:

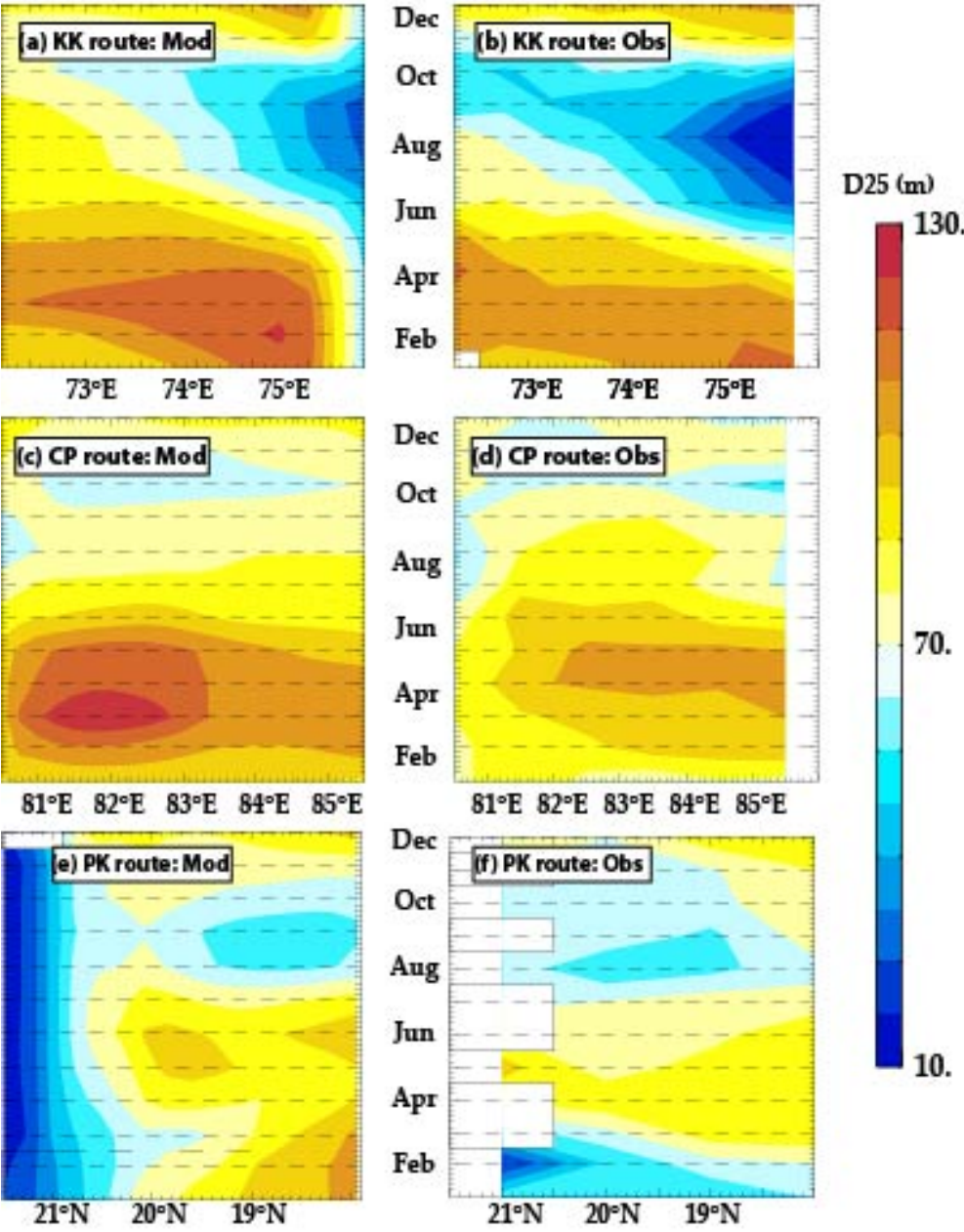


Figure 9:

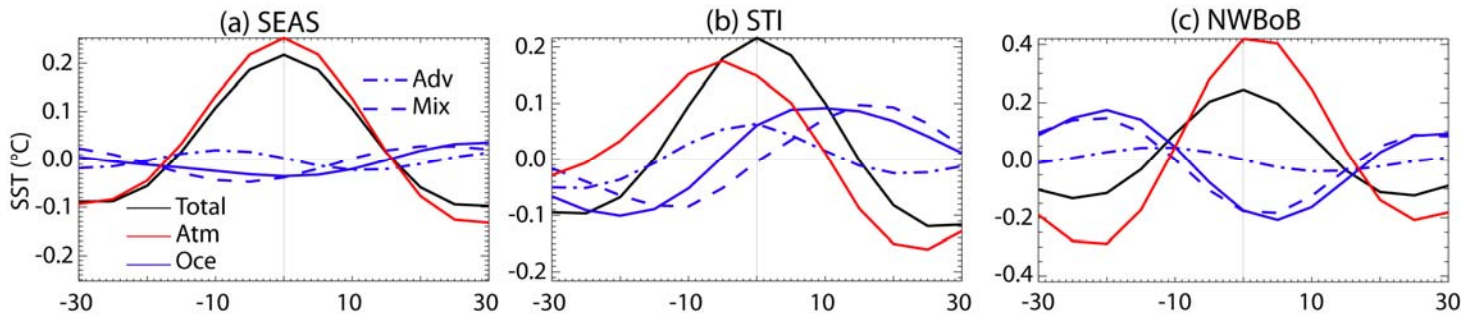


Figure 10:

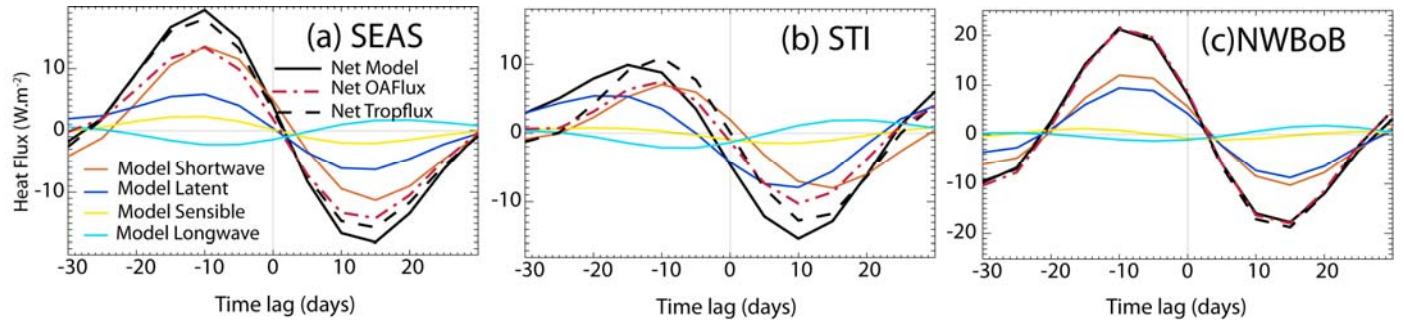


Figure 11:

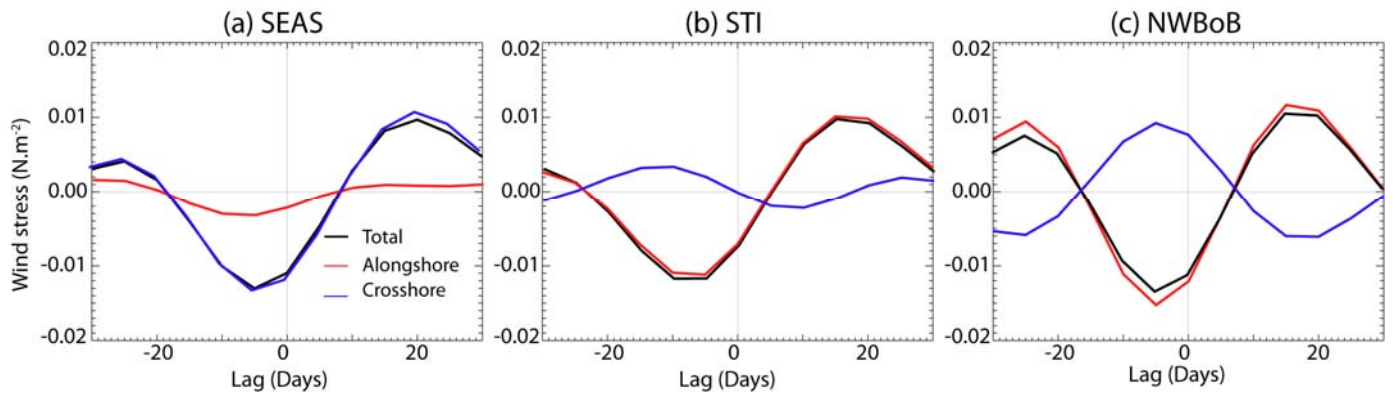


Figure 12:

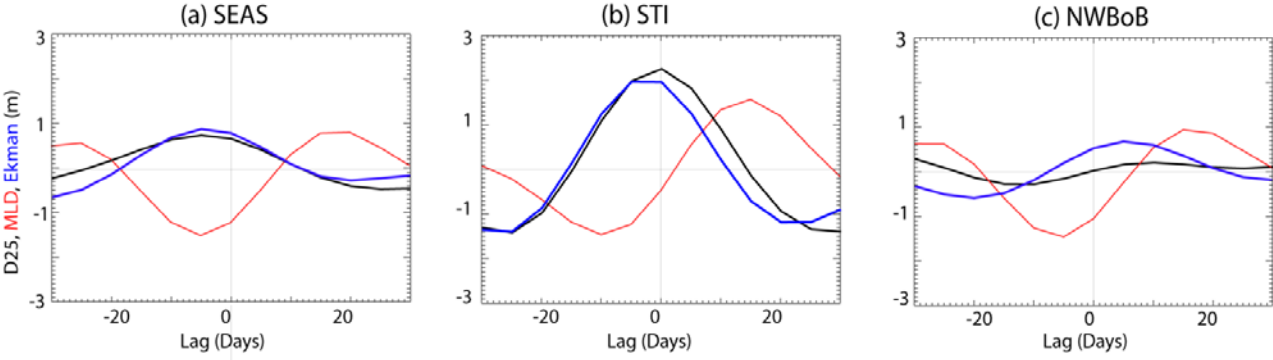


Figure 13:

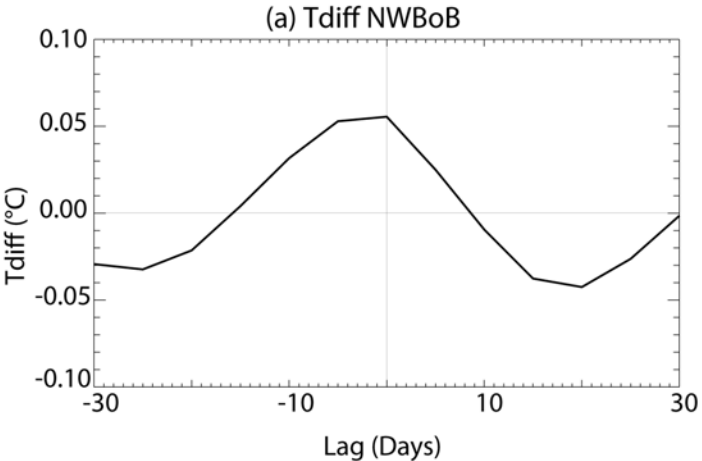


Figure 14:

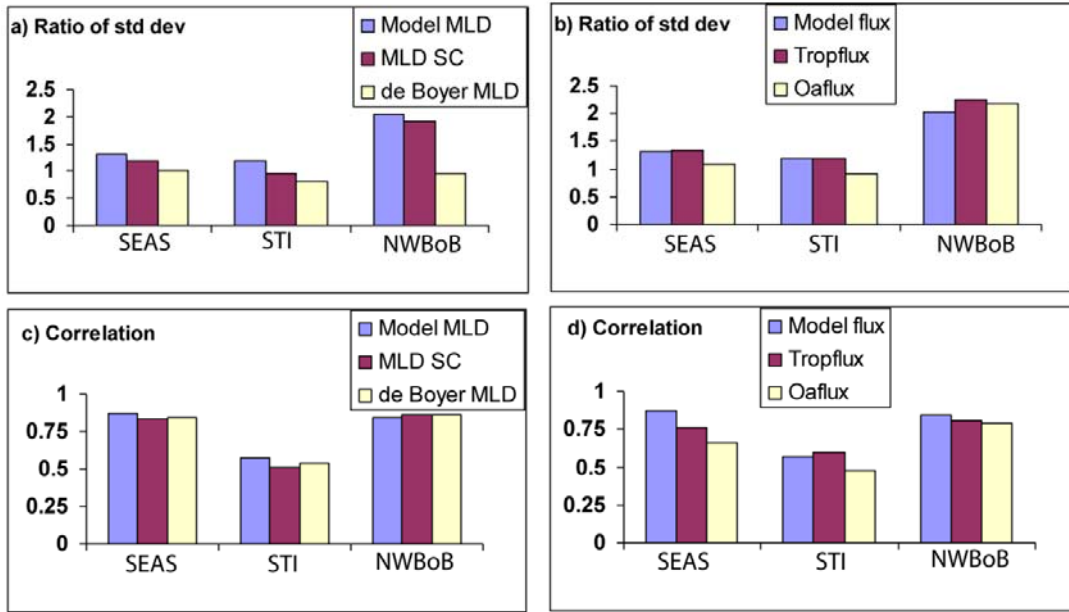


Figure 15:

